AIAA JOURNAL
Vol. 34, No. 11, November 1996

Leading-Edge Bluntness Effects in High Enthalpy, Hypersonic Compression Corner Flow

S. G. Mallinson,* S. L. Gai,† and N. R. Mudford‡
University of New South Wales, Canberra ACT 2600, Australia

An experimental study of the combined effects of leading-edge bluntness and real gas behavior on shock wave/boundary-layer interaction has been performed. Pressure and heat transfer distributions have been measured over a compression corner for a range of corner angles, including the datum case of flat plate flow. On the flat plate and upstream of the corner, the pressure and heat transfer for the blunt leading-edge configuration were found to lie above the corresponding sharp leading values. On the ramp, there was a considerable reduction in the pressure and heat transfer when the leading edge was blunt. Also, the extent of the interaction was seen to be smaller with the blunt leading edge. These results are similar to those from perfect gas studies. The differences between the sharp and blunt leading-edge data appear to be less pronounced at the higher enthalpy. This is thought likely to be because of the reduced shock standoff, which occurs as a result of dissociation. A comparison between the heat transfer data on the ramp face and predictions from the generalized reference enthalpy theory was seen to be reasonable. The upstream influence and plateau pressure were found to be in fair agreement with data from low enthalpy experiments.

Nomenclature

A = constant in Eq. (2)
C = Chapman–Rubesin constant, $(\mu/\mu_\infty)(T_\infty/T)$
C_D = drag coefficient
c = mole fraction
d = leading-edge thickness
h = enthalpy
h_r = recovery enthalpy, $h_0 + 0.5(Pr^{1/2} - 1)u_\infty^2$
L = upstream plate fetch
l_u = upstream influence
M = Mach number
m = Falkner–Skan pressure gradient parameter
n = exponent in generalized reference enthalpy theory
Pr = Prandtl number
p = pressure
q_w = heat transfer
Re_x = Reynolds number based on distance where x is $\rho_\infty U_\infty x/\mu_\infty$
Re_∞ = unit Reynolds number, $\rho_\infty U_\infty/\mu_\infty$
St = Stanton number, $q_w/[\rho_\infty U_\infty(h_r - h_w)]$
T = temperature
U = velocity
x = distance from leading edge
x_r = distance from the corner, $x - L$
α_O = oxygen dissociation fraction
β = combined bluntness-viscous interaction parameter, $\bar{\chi}_\varepsilon/\kappa_\varepsilon^{2/3}$
γ_f = frozen ratio of specific heats
δ = boundary-layer thickness
ε = $(\gamma - 1)/(\gamma + 1)$
ζ = Damkohler number, τ_d/τ_r
θ_w = corner angle
κ_ε = modified bluntness parameter, $\varepsilon M_\infty^3 C_D/(x/d)$
μ = viscosity
ρ = density
τ_d = characteristic particle diffusion time
τ_r = characteristic reaction time
ϕ = angular distance from the stagnation point
$\bar{\chi}_o$ = local hypersonic viscous interaction parameter, $M_o^3(C^*/Re_{x_o})^{1/2}$
$\bar{\chi}_\varepsilon$ = modified hypersonic viscous interaction parameter, $\varepsilon(0.664 + 1.73h_w/h_0)M_\infty^3(C^*/Re_x)^{1/2}$

Subscripts and Superscripts

g = gas phase value
N = nitrogen
O = oxygen
o = at the beginning of the interaction, x_o
p = plateau value
s = surface catalyzed value
w = conditions at the wall
0 = reservoir conditions
3 = conditions after expansion around the leading edge
∞ = freestream conditions
$*$ = evaluated at the Eckert reference enthalpy

Received Nov. 4, 1995; revision received May 22, 1996; accepted for publication May 24, 1996; also published in *AIAA Journal on Disc*, Volume 1, Number 4.

*Associate Lecturer, School of Aerospace and Mechanical Engineering, University College, Australian Defence Force Academy; currently Research Associate, Department of Aeronautics, Imperial College, Prince Consort Road, London SW7 2BY, England, United Kingdom. Member AIAA.

†Associate Professor, School of Aerospace and Mechanical Engineering, University College, Australian Defence Force Academy. Associate Fellow AIAA.

‡Lecturer, School of Aerospace and Mechanical Engineering, University College, Australian Defence Force Academy.

Introduction

HYPERSONIC vehicles may experience shock wave/boundary-layer interaction in their canopy and inlet regions and on their control surfaces. The interaction may cause the engine performance and control surface effectiveness to be reduced. It may also induce high heat loads. These factors need to be well understood when designing such a vehicle.

To reduce the heat loads near the vehicle nose and to allow installation of a cooling system, the leading edge of the vehicle must have some degree of bluntness.[1–3] A blunt leading edge gives rise to a high temperature layer of gas near the nose, called the entropy layer. The effects of the entropy layer are a lower Mach number, a lower unit Reynolds number, and fuller boundary layer velocity profiles, the latter a result of an induced favorable pressure gradient.[2,4] Thus, leading-edge bluntness may significantly alter the nature of the shock wave/boundary-layer interaction.

The compression corner is a convenient configuration for examining shock wave/boundary-layer interaction. It has been widely studied with both sharp[5–11] and blunt[4,12–16] leading edges. Blunting the leading edge has been found to increase the pressure and

heat transfer upstream of the corner, and to decrease them downstream of the corner, relative to the sharp leading-edge flows. For small leading-edge bluntness, separation is promoted and the transition location is moved downstream, whereas for large leading-edge bluntness, separation is delayed and the transition location is moved upstream. Small and large bluntness may be conveniently defined in terms of the combined bluntness-viscous interaction parameter β, where[4]

$$\beta = \bar{\chi}_\varepsilon / \kappa_\varepsilon^{2/3} \tag{1}$$

with $0.5 > \beta > 0.1$ for small leading-edge bluntness and $\beta \leq 0.1$ for large leading-edge bluntness. An examination of leading-edge bluntness effects using triple-deck theory has found essentially the same scaling laws.[14]

The flow over a hypersonic vehicle will typically be chemically reactive. The majority of investigations of the compression corner have considered perfect gas flow, with only a few experimental studies[17–19] and theoretical studies[20] examining the possible effects of real gas behavior. The experimental results seem to suggest that real gas effects are negligible for the conditions considered, whereas the theoretical studies predict significant differences between reacting and nonreacting flows. Computational studies of real gas effects for the more general problem of shock wave/boundary-layer interaction[21–27] predict the scale of interaction to be decreased when the overall real gas effect is endothermic (dissociation, vibrational excitation) and to be increased when the overall real gas effect is exothermic (recombination, vibrational relaxation). Even considering the aforementioned studies, there has been little if any attention paid to the combined effects of leading-edge bluntness and real gas effects on shock wave/boundary-layer interaction, in general, and compression corner flow, in particular.

Therefore, this paper examines the high enthalpy, hypersonic flow over a compression corner with blunt leading edges. Two leading-edge configurations were considered: hemicylindrical and square. Experiments have been conducted using a free-piston shock tunnel. The present data are compared with that from our previous studies of sharp leading-edge compression corner flow conducted under similar flow conditions.[18,19] The ramp heat transfer is analyzed in terms of a perfect gas theory modified to account for the presence of dissociated species in the flow. Also, important parameters such as the upstream influence and plateau pressure are examined in light of perfect gas theories, to see whether any real gas effect is evident.

Experimental Details

Facility and Test Flow Conditions

Experiments have been performed using the free-piston shock tunnel T3, located at the Australian National University.[28] Tests were performed at two conditions, designated B and G.[29] These have nozzle reservoir enthalpies of 18.0 and 2.8 MJ kg^{-1}, respectively.

The shock speed and nozzle reservoir pressure are obtained from records of pressure transducers mounted in the shock-tube side wall. These values, along with the shock-tube fill pressure and the chemical and thermophysical properties of the test gas, are input to a computational fluid dynamics (CFD) code,[30] which calculates the nozzle reservoir conditions. The nozzle flow is then calculated using nonequilibrium nozzle flow code,[31] with the input data consisting of the nozzle reservoir pressure and temperature and the chemical and thermophysical properties of the test gas. The conical nozzle employed in the present investigation has an inlet diameter of 12.7 mm, exit diameter of 305 mm, and a cone half-angle of 7.5 deg. The nozzle flow code is executed until the measured and calculated values of pitot pressure agree to within 1%. Extensive pitot pressure surveys[18] have found this to be equivalent to reducing the geometric conical half-angle to 7.3 deg for condition B and 6.9 deg for condition G and expanding to the actual axial location. This procedure has been adopted here.

Table 1 shows typical values of the reservoir and freestream conditions. The uncertainties in these conditions, because of the uncertainties in the input data and the nozzle flow divergence, are of the order ±5% for all of the parameters, except for the species concentrations, for which the uncertainty is less than ±1% (see Refs. 18 and 19). These uncertainties are of the same order as the shot-to-shot repeatability in the present facility. Further details on the calculation procedure used to determine these values are presented elsewhere.[18,19]

Conical nozzles can induce significant flow divergence effects, which may give rise to a favorable pressure gradient. To examine this, the Falkner–Skan pressure gradient parameter m was determined according to the method of Ref. 32. The axial variation in nozzle flow properties was taken as that calculated by nozzle flow code.[31] For conditions B and G, the value of m thus calculated was less than 0.01. This, along with the fact that pitot pressure surveys[18] revealed less than 1-deg flow divergence over the length of the model, suggest that flow divergence effects are negligible for the present experiments.

The free-piston shock tunnel has a short run time of the order 1 ms. This time may be reduced by driver gas contamination.[33] It has been found, however, that there is sufficient time to establish steady separated flow in a compression corner provided the reservoir enthalpy was less than approximately 20 MJ kg^{-1} (see Ref. 34).

Model and Instrumentation

The model employed in the present experiments is shown in Fig. 1a. It consisted of a flat plate with a detachable leading edge and a ramp plate. The model material was mild steel. These plates rested upon gauge housings. The corner angle was adjusted by inserting wedges beneath the housings. This paper will discuss results for corner angles of 0, 15, 18, and 24 deg.

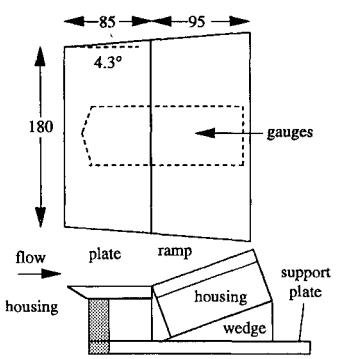

a) Model details

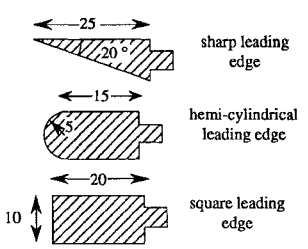

b) Leading-edge configurations

Fig. 1 Experimental model, showing detail of leading edge configurations (dimensions in millimeters).

Table 1 Typical reservoir and freestream conditions

	h_0, MJ kg^{-1}	p_0, MPa	T_0, K	p_∞, kPa	T_∞, K	ρ_∞, g m^{-3}	U_∞, km s^{-1}	M_∞,	Re_∞ × 10^{-5}, m^{-1}	$\gamma_{f\infty}$	α_0	β,[a] h.l.e.[b]	β, s.l.e.[c]
B	18.0	20.0	8100	0.85	1080	2.50	5.30	7.5	2.80	1.45	0.8	0.07	0.05
G	2.78	22.0	2300	0.65	150	16.0	2.30	9.1	31.0	1.40	0.0	0.03	0.02

[a]Values of β calculated at the hinge line, $x = 80$ mm. [b]Hemicylindrical leading edge. [c]Square leading edge.

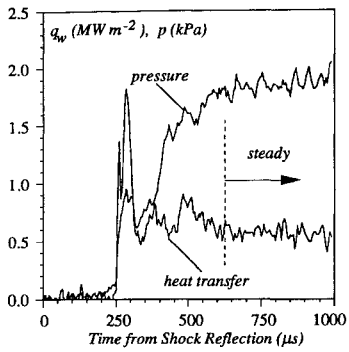

Fig. 2 Typical unfiltered pressure and heat transfer records (condition B). Similar results are obtained for condition G.

Upwash from underneath the model was prevented by side skirts. Leakage through the corner was prevented by sealing from below with an industrial sealing compound.

The model aspect ratio was slightly greater than 1 to ensure two dimensionality in the model midspan region.[8] A numerical investigation of nominally two-dimensional compression corner flow[35] indicated that three-dimensional effects may be present even for flows that satisfy the criterion of Ref. 8. Although it has been found that the study of Ref. 35 was not conclusive,[36] it is nevertheless important to examine the possibility of three-dimensional effects. The heat transfer and pressure were measured at an axial location within the separated region both on- and off-centerline of the model. It was felt that three-dimensional effects would be more pronounced in the separated region and so these measurements would indicate the extent to which three-dimensional effects would affect the results. These tests were repeated with side fences to prevent spillage from the separated region. The side fences extended to just downstream of the nose to just upstream of the trailing-edge of the model. The height of the fences was always at least greater than the local boundary-layer thickness. The differences between data from on- and off-centerline locations and from tests with and without side fences were well within the gauge uncertainty and hence negligible. This suggests that the flow in the model midspan region may be considered to be nominally two dimensional.

Two blunt leading edges were employed: hemicylindrical and square. The nose drag coefficients for these leading edges are $C_D = \frac{4}{3}$ and 2, respectively.[37] These values are strictly valid for perfect gas flows only, but serve as a reasonable first approximation for the high enthalpy condition B employed here. The sharp leading edge used in the previous experiments[18,19] satisfied the sharpness criterion proposed by Stollery.[38] The three leading edges are shown in Fig. 1b.

The surface pressure and temperature were measured using PCB 113M165 pressure transducers and coaxial chromel-alumel (type K) thermocouples, respectively. Up to 12 pressure transducers and 20 thermocouples could be employed in a single run. However, not all of the gauges were employed in every run because of problems with the data collection system. The heat transfer was obtained from the temperature variation with time, according to Ref. 39. Typical pressure and heat transfer records are shown in Fig. 2. Using the method described in Ref. 40, the thermocouple thermal product was determined to be 9500 ± 500 W s$^{1/2}$ m^{-2} K^{-1}. The uncertainty in the measurements from these gauges is ±10 and ±15%, for the pressure and heat transfer, respectively.[18,41]

Ramp Face Heat Transfer Modeling for Blunt Leading-Edge Compression Corner Flow

The ramp face heat transfer may be analyzed in terms of the generalized reference enthalpy theory. For flow in a pressure gradient, this theory gives the heat transfer as[42]

$$St Re_{x_r}^n = \frac{A}{Pr^{2/3}} \left(\frac{U_e p_e}{U_\infty p_\infty}\right)^{(1-n)} \left(\frac{T_\infty}{T^*}\right)^{(1-2n)} (C^*)^n \frac{(h_r - h_w)}{(h_0 - h_w)} \tag{2}$$

where $A = 0.332$ and $n = 0.5$ for laminar flow and $A = 0.0296$ and $n = 0.2$ for turbulent flow.

Despite the fact that this model was originally intended for use in attached flows only, it has been successfully employed to predict the heat transfer to the ramp face for attached and separated flow of a perfect gas over sharp and blunt leading-edge compression corners.[12,16] In the latter study, the pressure external to the boundary layer, p_e, was taken as the measured wall pressure. The other conditions were evaluated by assuming an isentropic expansion from just behind the corner shock to the measured pressure. The distance x_r was measured from the corner.[16]

Table 2 Flow conditions after end of nose expansion

Condition, leading edge	$\{1 - [h_{chem}/(h_r - h_w)]\}$	c_N	c_O	M_3
B, hemicylindrical	0.72	0.035	0.229	3.20
B, square	0.71	0.036	0.229	3.30
G, hemicylindrical	1	0	0	2.94
G, square	1	0	0	2.95

For condition B, a simple perfect gas calculation of the flow in the nose region will not suffice. It is important to include the effect of the dissociation behind the leading edge bow shock and the recombination through the expansion around the nose. To do this, the pressure distribution has been taken as that given by the modified-Newtonian expression for the hemicylindrical nose[1] and an expression from Probstein[43] for the square leading edge. It is further assumed that the flow expands from $\phi = 60$ deg for the hemicylindrical leading edge, and from the corner for the square leading edge, to the measured pressure on the flat plate. The flow through these specified pressure distributions may be calculated using a CFD code for nonequilibrium expansions.[31] The full details of this calculation are presented elsewhere.[18]

The important flow parameters after the expansion around the leading edge are given for condition B in Table 2. Also shown are the parameters for condition G, evaluated assuming perfect gas flow.

The local flow conditions on the ramp face may be evaluated by taking the Mach number given in Table 2 and calculating the flow through the oblique shock at the corner. The flow through this shock can be assumed to be frozen as the flow lengthscale is much smaller than any reaction lengthscale. Also, for the angles considered here, the shock will be weak. Using the value of the Mach number behind the shock, the local conditions may be calculated by assuming an isentropic expansion to the measured pressure on the ramp face.

For condition B, the presence of dissociated species in the flow may reduce the heat transfer below the levels predicted by Eq. (2). This gives rise to two limits for the heat transfer: 1) the equilibrium limit, where complete recombination of the dissociated species occurs at or before the wall, and 2) the frozen limit, where there is no chemical activity. The equilibrium limit is given by Eq. (2). The frozen limit for the ramp face heat transfer will be given by Eq. (2) multiplied by $[1 - h_{chem}/(h_r - h_w)]$, which is shown in Table 2. Here, h_{chem} is the chemical potential enthalpy of the dissociated species. Note that for condition G, $h_{chem} = 0$ and so the two limits are identical.

Results

Flat Plate (θ_w = 0 deg)

The configuration where the corner angle is zero is equivalent to a flat plate and is the datum for compression corner flow.

The pressure and heat transfer distributions for the flat plate with hemicylindrical and square leading edges are compared with each other and with the corresponding sharp leading-edge data[18,19] in Figs. 3 and 4, respectively. The typical error bars shown represent ±10% for the pressure and ±15% for the heat transfer. The lack of data points for the pressure distributions past the corner ($x/L > 1$) for some runs is a result of gauge failure.

First consider the pressure. For the high enthalpy condition B, the blunt leading-edge data seem to lie closer to the sharp leading-edge data than is the case for the low enthalpy condition G. Also, there seems to be less difference between the hemicylindrical and square leading-edge data for condition B than for condition G.

Now consider the heat transfer. It is seen that the data for the square leading edge lie above both the hemicylindrical and sharp

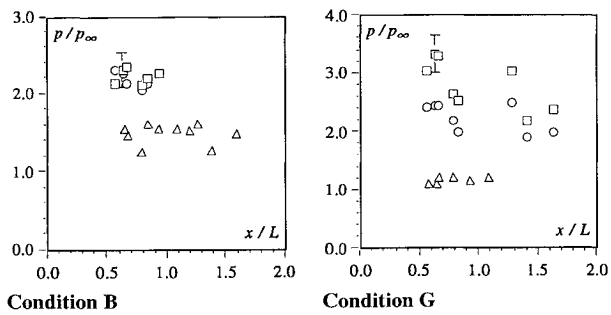

Fig. 3 Flat plate pressure distributions: △, sharp leading edge; ○, hemicylindrical leading edge; and □, square leading edge.

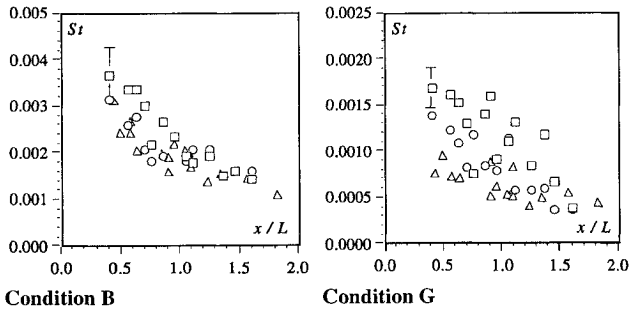

Fig. 4 Flat plate heat transfer distributions; refer to Fig. 3 for an explanation of the symbols.

leading-edge data. This difference is more pronounced for condition G. In fact, the sharp leading-edge data could be said to be indistinguishable from the hemicylindrical leading-edge data for condition B.

From these pressure and heat transfer distributions, it may be said that the difference between the sharp and blunt leading-edge flows was more pronounced at low enthalpy. This may be because of the reduced shock stand-off experienced under high enthalpy conditions.[44,45] This would lead to a thinner entropy layer and, hence, a smaller leading-edge bluntness effect.

The flat plate boundary layer for the sharp leading-edge flow has been found to be laminar.[18,19] For the blunt leading-edge flat plate, the heat transfer does not exhibit the strong rise because of transition to turbulence and the traces of pressure and heat transfer do not exhibit characteristic unsteadiness associated with transition to turbulence. Also, as will be seen in the following section, the heat transfer upstream of the corner is seen to decrease for corner angles $\theta_w > 0$ deg. These observations would tend to indicate that the flow is laminar for the blunt flat plate flow. Whether this remains the case for the compression corner will be examined in the following sections.

Compression Corner ($\theta_w > 0$ deg)

The pressure and heat transfer distributions for conditions B and G at corner angles of 15, 18, and 24 deg are shown in Figs. 5 and 6 for hemicylindrical and square leading-edge compression corners, along with corresponding data from sharp leading-edge experiments.[18,19] The typical error bars shown represent ±10% for the pressure and ±15% for the heat transfer. For some tests, the error bars are smaller than the points themselves and are therefore not visible.

It is clear that the pressure and heat transfer on the ramp face for the blunt leading-edge configuration are lower than that for the sharp leading edge. Overall, there does not seem to be much difference between the levels of pressure and heat transfer on the ramp face for the hemicylindrical and square leading-edge configurations. Also, the upstream influence seems to be decreased whereas the plateau pressure seems to be increased by blunting the leading edge. These aspects of compression corner flow will now be examined in further detail.

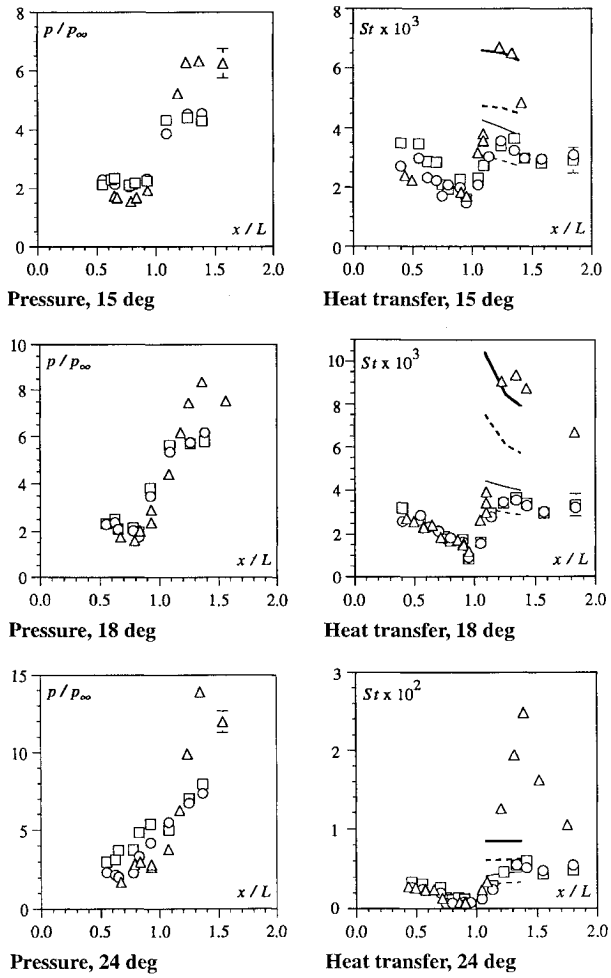

Fig. 5 Pressure and heat transfer distributions for compression corner, condition B: △, sharp leading edge; ○, hemicylindrical leading edge; and □, square leading edge. Curves indicate predictions for blunt leading-edge flows: light solid curve, equilibrium limit, laminar flow; light dashed curve, frozen limit, laminar flow; heavy solid curve, equilibrium limit, turbulent flow; and heavy dashed curve, frozen limit, turbulent flow.

Ramp Face Heat Transfer

The predictions for equilibrium and frozen limits for both laminar and turbulent flow obtained from Eq. (2) are shown in Figs. 5 and 6. Note that the data scatter is of the same order as the difference between the frozen and equilibrium limits. It would seem that the ramp heat transfer for condition B lies between the frozen and equilibrium limits for laminar flow at 15 deg, tending toward the equilibrium laminar limit as the ramp angle is increased. The condition B data lie below the frozen limit for turbulent flow for $\theta_w = 15$ and 18 deg, indicating that the flow remains laminar; for $\theta_w = 24$ deg, the data appear to be within the experimental scatter of both laminar and turbulent predictions. As the heat transfer and pressure traces do not exhibit the characteristic unsteadiness of turbulent flows, it would seem unlikely that transition has occurred here.

The Damkohler number ζ is the ratio of the characteristic times for molecular diffusion and chemical reaction. For $\zeta \ll 1$, chemical reactions proceed slowly and the flow is said to be chemically frozen; for $\zeta \gg 1$, chemical reactions proceed rapidly and the flow is said to be in chemical equilibrium. When $\zeta = \mathcal{O}(1)$, nonequilibrium effects are important. By evaluating ζ for gas-phase and surface-catalyzed recombination, it may be possible to determine whether the measured heat transfer should correspond to frozen, nonequilibrium, or equilibrium flow. Here, ζ_g and ζ_s will be calculated for nitrogen and oxygen recombination according to Ref. 46. The gas-phase recombination rates are taken from Ref. 29, whereas the surface catalycity is taken as that for iron, which is given by Ref. 47 as $k_w \approx 5$ m s^{-1}

Table 3 Damkohler number for gas-phase and surface-catalyzed recombination on the ramp face for condition B, blunt leading edge (x_r = 45 mm)

Corner angle, θ_w, deg	ζ_g (nitrogen)	ζ_g (oxygen)	ζ_s (nitrogen and oxygen)
15	1.6×10^{-2}	1.5×10^{-3}	0.43
18	1.8×10^{-2}	1.7×10^{-3}	0.49
24	2.8×10^{-2}	2.7×10^{-3}	0.61

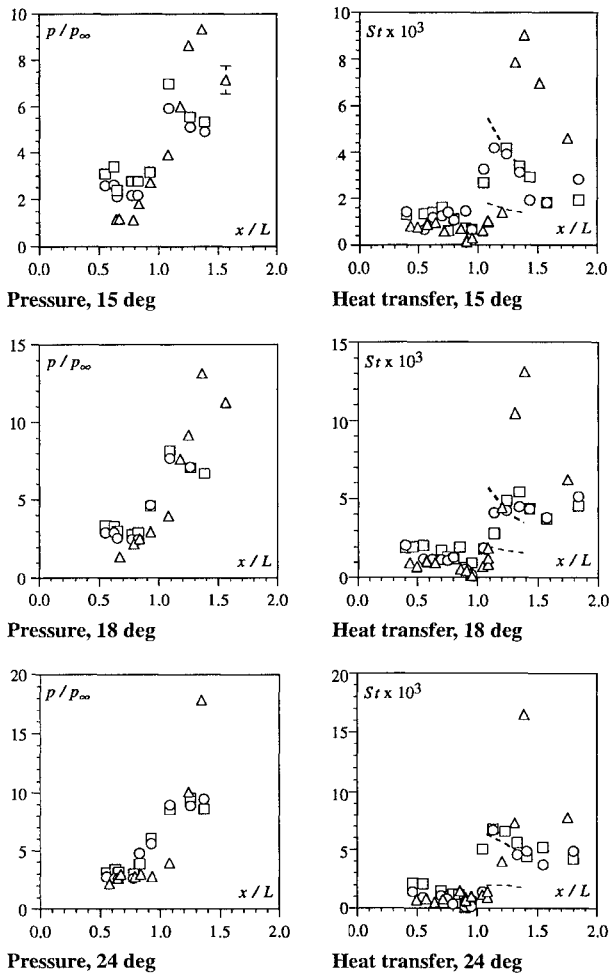

Fig. 6 Pressure and heat transfer distributions for compression corner, condition G; refer to Fig. 5 for an explanation of the symbols.

for both nitrogen and oxygen. The values of ζ_g and ζ_s halfway along the ramp face ($x_r = 45$ mm) are shown in Table 3 for condition B at the three corner angles tested. For condition G, there are only trace levels of atomic species present in the flow; regardless, the flow is nonreactive for this condition.

The values in Table 3 suggest that, for condition B, gas-phase recombination is close to frozen, whereas surface-catalyzed recombination is in nonequilibrium. Also, as the corner angle is increased, both gas-phase and surface-catalyzed recombination appear to become more important and, thus, the heat transfer should tend toward equilibrium. It is not possible to say whether the equilibrium heat transfer limit is reached at condition B, especially given the scatter in the data.

For condition G the blunt leading-edge ramp face heat transfer appears to compare reasonably well with the prediction for the frozen limit of blunt leading-edge turbulent flow at all three ramp angles tested. For the sharp leading edge, the flow appears to remain laminar throughout the interaction for conditions B and G.[18,19] It is thus possible that for condition G, transition to turbulence may have been shifted upstream relative to the sharp leading-edge configuration. Certainly, the heat transfer on the flat plate upstream of the corner decreases for both sharp and blunt leading-edge flows, which is characteristic of laminar separation. It would therefore seem likely that if transition to turbulence is occurring for the blunt leading-edge flows at condition G, it does so near to reattachment. The upstream shift in the location of transition is consistent with previous studies given the large bluntness indicated by the values of β (see Table 1).

Note that the use of the simple correlation of Eq. (2) to predict the heat transfer on the ramp face for the blunt leading-edge flows is not a substitute for more elaborate methods such as the full Navier–Stokes equations along with a Reynolds stress turbulence model. Thus, only tentative conclusions may be drawn from comparison of experimental data with this model.

Upstream Influence

The upstream influence l_u may be defined as the distance upstream of the corner where the pressure or heat transfer first deviates from the flat plate distribution. It is a useful means of examining separation in shock wave/boundary-layer interaction. Upon close examination of Figs. 5 and 6, it would appear that the upstream influence is reduced for the blunt leading-edge flows. This is consistent with the large leading-edge bluntness indicated by the values of β for conditions B and G (see Table 1).

It has been found that the upstream influence in hypersonic laminar flow over sharp leading-edge compression corners is fairly well described in terms of the following expression[18,19]:

$$\frac{l_u}{\delta_o} = F\left[\frac{(M_o\theta_w)^2}{\bar{\chi}_o}\right] \tag{3}$$

Data for sharp leading-edge compression corner experiments at the high and low enthalpy conditions of current interest and other low enthalpy data have been found to compare well in this form, indicating that the real gas effects on separation are small for the sharp leading-edge flows.[18,19] This expression contains terms that depend only on the corner angle and the conditions at the edge of the boundary layer. It is therefore tempting to apply Eq. (3) to blunt leading-edge compression corner flows.

Figure 7 shows the upstream influence data from the present experiments, along with data from our previous sharp leading-edge studies[18,19] and some data from perfect gas studies performed with sharp[5–11] and blunt[13,16] leading edges. For the present experiments, the flow was deemed to be separated if the surface pressure had a plateau in the distribution near the corner or if the heat transfer had a cuspid, as opposed to sharp, minimum near the corner. These criteria were also applied to the other studies. In some of the other studies, skin friction and flow visualization data were also presented, and so it was possible to determine whether the flow was separated in those cases by determining if the skin friction had passed below zero, or by examining the flow visualization data. For the present flow conditions B and G, the flow parameters at the edge of the boundary

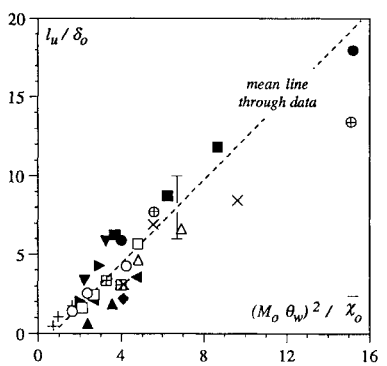

Fig. 7 Upstream influence in hypersonic compression corner flows: comparison between sharp and blunt leading-edge flows. The condition D experiments with the sharp leading edge had a reservoir enthalpy $h_0 \approx 14$ MJ kg^{-1} (see Refs. 18 and 19): ○, condition B, sharp[19]; □, condition D, sharp[19]; △, condition G, sharp[19]; +, condition B, blunt; ×, condition G, blunt; ●, sharp[5]; ■, sharp[6]; ▲, sharp[7]; ▼, sharp[8]; ◄, sharp[9]; ►, sharp[10]; ♦, sharp[11]; ⊞, blunt[13]; and ⊕, blunt[16].

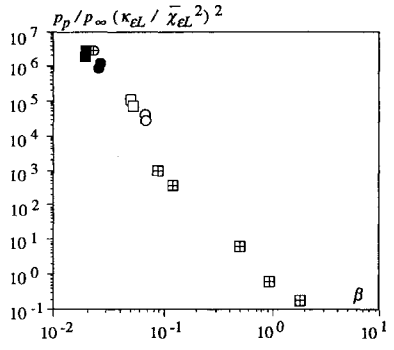

Fig. 8 Correlation of plateau pressure for blunt leading-edge compression corner flow: ○, B, hemicylindrical; □, B, square; ●, G, hemicylindrical; ■, G, square; ⊞, hemicylindrical and square[4]; and ⊕, hemicylindrical.[16]

layer were obtained in the manner described earlier for the ramp face heat transfer modeling. For all of the points, the value of δ_O was calculated using an expression that compares reasonably well with experimental data from high and low enthalpy flows.[18,19]

The error bar shown in Fig. 7 represents ±25%, which is typical of the scatter at the point shown. For smaller upstream influence, it is more difficult to evaluate the exact value of l_u and so the scatter in data is greater, as is evident from Fig. 7. Nevertheless, it is seen that all of the data—sharp and blunt leading edge, low and high enthalpy—appear to compare quite well amongst themselves. Two of the points, one from the present condition G experiments, the other from Ref. 16, are somewhat below the other data. This may be because of the flow undergoing transition to turbulence upstream of the corner for these flows.

The comparison in Fig. 7 suggests that 1) leading-edge bluntness effects on upstream influence can be accounted for by examining the interaction in terms of local variables just upstream of the interaction and 2) provided the real gas effects near the nose are included when determining the conditions external to the boundary layer, there does not seem to be any further real gas or bluntness effect on upstream influence. The latter is consistent with calculations of the characteristic reaction lengthscales in the blunt leading-edge condition B experiments, which reveal the flow to be chemically frozen.[18]

Plateau Pressure

The plateau pressure is another means of examining separation in shock wave/boundary-layer interaction. It has been found for perfect gas flow over blunt leading-edge compression corners that the plateau pressure may be expressed as[4]

$$(p_p/p_\infty)\left(\kappa_{\varepsilon_L}/\bar{\chi}_{\varepsilon_L}^2\right)^2 = F(\beta) \tag{4}$$

The plateau pressure data from the present experiments are compared in Fig. 8, along with experimental data from two previous studies of blunt leading-edge compression corner flow at low enthalpy.[4,16] It appears that there is good agreement between the high and low enthalpy data, which suggests that the real gas effect on the plateau pressure is small for the present experimental conditions. As a final point, note that the data shown in Fig. 8 appear to be clustered around different pressure levels, with the changeover in slope occurring near $\beta = 0.1$, that is, the border between small and large bluntness.

Conclusions and Summary

The combined effects of leading-edge bluntness and real gas effects on flat plate and compression corner flow have been examined.

For the flat plate, the pressure and heat transfer lie above the sharp leading-edge values, which is consistent with previous studies under perfect gas conditions. The difference between sharp and blunt leading-edge flows seems to be more pronounced at low enthalpy. This may be attributed to the smaller bow shock stand off, which occurs due to dissociation, reducing the effect of leading-edge bluntness at high enthalpy.

For the compression corner, the pressure and heat transfer on the ramp face and the scale of the interaction were reduced, and the plateau pressure increased, which is in accordance with the previous studies performed under perfect gas conditions with similar values of the combined viscous-bluntness parameter β.

The ramp face heat transfer for the blunt leading-edge flows was examined in terms of the modified reference enthalpy theory, which includes pressure effects. For the high enthalpy flow condition B, the heat transfer on the ramp face for the blunt leading-edge configurations appeared initially to be closer to the prediction for frozen laminar flow, tending toward the equilibrium laminar limit as the ramp angle was increased. This was in qualitative agreement with the calculated values of gas-phase and surface-catalyzed Damkohler numbers for this condition. For the low enthalpy flow condition G, the ramp face heat transfer data for the blunt leading-edge configurations seemed to be in good agreement with the prediction for frozen turbulent flow. This suggests that the introduction of leading-edge bluntness may lead to an upstream movement of transition relative to the sharp leading-edge configuration for this condition. Although this is consistent with previous studies conducted under perfect gas conditions with similar values of β, further detailed studies are required to examine the effect of bluntness on transition to turbulence.

The upstream influence for the present experiments was found to be reasonably well described by a correlation previously used for high and low enthalpy flow over compression corners with sharp leading edges. For condition B, the flow parameters at the edge of the boundary layer were determined by including the effects of chemical reactions, whereas for condition G, a perfect gas calculation sufficed. Also, the plateau pressure data were seen to compare quite well with previous low enthalpy data in terms of a combined bluntness-viscous similitude. It would therefore appear that once the real gas effects in the nose region are accounted for, the flow behaved essentially as a perfect gas upstream of the corner.

Acknowledgment

The authors would like to thank P. M. Walsh for technical assistance with the experiments.

References

[1]Lees, L., "Laminar Heat Transfer over Blunt-Nosed Bodies at Hypersonic Flight Speeds," *Jet Propulsion*, Vol. 26, No. 4, 1956, pp. 259–269, 274.

[2]George, A. R., "Perturbations of Plane and Axisymmetric Entropy Layers," *AIAA Journal*, Vol. 5, No. 12, 1967, pp. 2155–2160.

[3]Blosser, M. L., Blankson, I. M., Schwoerke S., Brunson, D., and Hagseth, P., "Wing Leading-Edge Design Concepts for Airbreathing Hypersonic Waveriders," *Journal of Aircraft*, Vol. 32, No. 2, 1995, pp. 307–312.

[4]Holden, M. S., "Boundary-Layer Displacement and Leading-Edge Bluntness Effects on Attached and Separated Laminar Boundary Layers in a Compression Corner. Part II: Experimental Study," *AIAA Journal*, Vol. 9, No. 1, 1971, pp. 84–93.

[5]Putnam, L. E., "Investigation of Effects of Ramp Span and Deflection Angle on Laminar Boundary-Layer Separation at Mach 10.03," NASA TN D-2833, May 1965.

[6]Needham, D. A., and Stollery, J. L., "Hypersonic Studies of Incipient Separation and Separated Flows," *AGARD Conference Proceedings*, Vol. 4, Pt. 1, 1966, pp. 89–119.

[7]Holden, M. S., "Experimental Studies of Separated Flows at Hypersonic Speeds. Part II: Two-Dimensional Wedge Separated Flow Studies," *AIAA Journal*, Vol. 4, No. 5, 1966, pp. 790–799.

[8]Lewis, J. E., Kubota, T., and Lees, L., "Experimental Investigation of Supersonic Laminar, Two-Dimensional Boundary-Layer Separation in a Compression Corner With and Without Cooling," *AIAA Journal*, Vol. 6, No. 1, 1968, pp. 7–14.

[9]Holden, M. S., and Moselle, J. R., "Theoretical and Experimental Studies of the Shock Wave-Boundary Layer Interaction on Compression Surfaces in Hypersonic Flow," Aeronautical Research Lab., ARL Rept. 70-0002, U.S. Air Force, Wright–Patterson AFB, OH, Jan. 1970.

[10]Bloy, A. W., and Georgeff, M. P., "The Hypersonic Laminar Boundary Layer Near Sharp Compression and Expansion Corners," *Journal of Fluid Mechanics*, Vol. 63, Pt. 3, 1974, pp. 431–447.

[11]Grasso, F., Leone, G., and Délery, J. M., "Validation Procedure for the Analysis of Shock-Wave/Boundary-Layer Interaction Problems," *AIAA Journal*, Vol. 32, No. 9, 1994, pp. 1820–1827.

[12]Vermeulen, J. P., and Simeonides, G., "Parametric Studies of Shock Wave/Boundary Layer Interactions over 2D Compression Corners at Mach 6," von Kármán Inst., TN 181, Rhode-St Genèse, Belgium, Sept. 1992.

[13]Coët, M.-C., Délery, J., and Chanetz, B., "Experiments on Shock Wave—Boundary Layer Interaction at High Mach Number with Entropy Layer Effect," *Proceedings of the IUTAM Symposium: Aerothermochemistry of Spacecraft and Associated Hypersonic Flows* (Marseille, France), 1992, Jouve, Paris, France, pp. 338–343.

[14]Lagrée, P. Y., "Influence of the Entropy Layer on Viscous Triple Deck Hypersonic Scales," *Proceedings of the IUTAM Symposium: Aerothermochemistry of Spacecraft and Associated Hypersonic Flows* (Marseille, France), 1992, pp. 358–361.

[15]Kumar, D., and Stollery, J. L., "Effects of Leading Edge Bluntness on Control Flap Effectiveness at Hypersonic Speeds," *Proceedings of the 19th International Symposium on Shock Waves* (Marseille, France), Springer–Verlag, Berlin, 1993, Vol. 1, pp. 47–52.

[16]Kumar, D., and Stollery, J. L., "Hypersonic Control Flap Effectiveness," 19th Congress of the International Council of Aeronautical Sciences, ICAS Paper 94-4.4.3, Sept. 1994.

[17]Stalker, R. J., and Rayner, J. P., "Shock Wave-Laminar Boundary Layer Interaction at Finite Span Compression Corners," *Proceedings of the 15th International Symposium on Shock Waves and Shock Tubes*, Stanford Univ. Press, Stanford, CA, 1985, pp. 509–515.

[18]Mallinson, S. G., "Shock Wave/Boundary Layer Interaction at a Compression Corner in Hypervelocity Flows," Ph.D. Thesis, Dept. of Aerospace and Mechanical Engineering, Univ. College, Univ. of New South Wales, Canberra, Australia, 1994.

[19]Mallinson, S. G., Gai, S. L., and Mudford, N. R., "High Enthalpy, Hypersonic Compression Corner Flow," AIAA Paper 95-0155, Jan. 1995.

[20]Grasso, F., and Leone, G., "Chemistry Effects in Shock Wave Boundary Layer Interaction," *Proceedings of the IUTAM Symposium: Aerothermochemistry of Spacecraft and Associated Hypersonic Flows* (Marseille, France), Jouve, Paris, France, 1992, pp. 220–227.

[21]Ballaro, C. A., and Anderson, J. D., Jr., "Shock Strength Effects on Separated Flows in Non-Equilibrium Chemically Reacting Air Shock Wave/Boundary Layer Interaction," AIAA Paper 91-0250, Jan. 1991.

[22]Brenner, G., and Prinz, U., "Numerical Simulation of Chemical and Thermal Nonequilibrium Flows After Compression Shocks," AIAA Paper 92-2879, July 1992.

[23]Kordulla, W., Riedelbauch, S., Brenner, G., and Prinz, U., "Hypersonic Viscous Flow Simulation," *Fluid Dynamics Research*, Vol. 10, 1992, pp. 451–468.

[24]Yungster, S., "Numerical Study of Shock-Wave/Boundary-Layer Interactions in Premixed Combustible Gases," *AIAA Journal*, Vol. 30, No. 10, 1992, pp. 2379–2387.

[25]Brenner, G., Gerhold, T., Hannemann, K., and Rues, D., "Numerical Study of Shock/Shock and Shock-Wave/Boundary-Layer Interactions in Hypersonic Flows," *Computers and Fluids Journal*, Vol. 22, No. 4/5, 1993, pp. 427–439.

[26]Grumet, A., Anderson, J. D., Jr., and Lewis, M. J., "Numerical Study of the Effects of Wall Catalysis on Shock Wave/Boundary Layer Interaction," *Journal of Thermophysics and Heat Transfer*, Vol. 8, No. 1, 1994, pp. 40–47.

[27]Oswald, J., Demargne, A., and Bousquet, J.-M., "Hypersonic Laminar Computations of Separated Flows with Account of Real Gas Effects," AIAA Paper 95-2271, June 1995.

[28]Stalker, R. J., "Development of a Hypervelocity Wind Tunnel," *Aeronautical Journal*, Vol. 76, June 1972, pp. 374–384.

[29]East, R. A., Stalker, R. J., and Baird, J. P., "Measurements of Heat Transfer to a Flat Plate in a Dissociated High-Enthalpy Laminar Air Flow," *Journal of Fluid Mechanics*, Vol. 97, No. 4, 1980, pp. 673–699.

[30]McIntosh, M. K., "A Computer Program for the Numerical Calculation of Equilibrium and Perfect Gas Conditions in Shock Tunnels," Australian Defence Scientific Service, WRE TN CPD 169, Salisbury, Australia, April 1970.

[31]Lordi, J. A., Mates, R. E., and Moselle, J. R., "Computer Program for the Numerical Solution of Nonequilibrium Expansions of Reacting Gas Mixtures," NASA CR-472, 1966.

[32]Cohen, C. G., and Reshotko, E., "Similar Solutions for the Compressible Laminar Boundary Layer with Heat Transfer and Pressure Gradient," NACA Rept. 1293, 1956.

[33]Crane, K. C. A., and Stalker, R. J., "Mass-Spectrometric Analysis of Hypersonic Flows," *Journal of Physics D: Applied Physics*, Vol. 10, No. 5, 1977, pp. 679–695.

[34]Mallinson, S. G., and Gai, S. L., "Establishment of Laminar Separated Flows in a Free-Piston Shock Tunnel," *Proceedings of the IUTAM Symposium: Aerothermochemistry of Spacecraft and Associated Hypersonic Flows* (Marseille, France), Jouve, Paris, France, 1992, pp. 368–373.

[35]Rudy, D. H., Thomas, J. L., Kumar, A., Gnoffo, P. A., and Chakravarthy, S. R., "Computation of Laminar Hypersonic Compression-Corner Flows," *AIAA Journal*, Vol. 29, No. 7, 1991, pp. 1108–1113.

[36]Lee, J. Y., and Lewis, M. J., " Numerical Study of the Flow Establishment Time in Hypersonic Shock Tunnels," *Journal of Spacecraft and Rockets*, Vol. 30, No. 2, 1993, pp. 152–163.

[37]Anderson, J. D., Jr., *Hypersonic and High Temperature Gas Dynamics*, McGraw–Hill, New York, 1989.

[38]Stollery, J. L., "Viscous Interaction Effects on Re-Entry Aerothermodynamics: Theory and Experimental Results," *Aerodynamic Problems of Hypersonic Vehicles*, AGARD Lecture Series 42, Vol. 1, 1972.

[39]Schultz, D. L., and Jones, T. V., "Heat-Transfer Measurements in Short-Duration Hypersonic Facilities," AGARDograph 165, 1973.

[40]Jessen, C., Vetter, M., and Grönig, H., "Experimental Studies in the Aachen Hypersonic Shock Tunnel," *Zeitschrift für Flugwissenschaften und Weltraumforschung*, Vol. 17, No. 2, 1993, pp. 73–81.

[41]Gai, S. L., and Joe, W. S., "Laminar Heat Transfer to Blunt Cones in High-Enthalpy Hypervelocity Flows," *Journal of Thermophysics and Heat Transfer*, Vol. 6, No. 3, 1992, pp. 433–438.

[42]Neumann, R. D., and Hayes, J. R., "Introduction to Aerodynamic Heating Analysis of Supersonic Missiles," *Tactical Missile Aerodynamics*, edited by M. J. Hemsch and J. N. Nielsen, Vol. 104, Progress in Astronautics and Aeronautics, AIAA, New York, 1986, pp. 421–481.

[43]Probstein, R. F., "Inviscid Flow in the Stagnation Point Region of Very Blunt-Nosed Bodies at Hypersonic Flight Speeds," Brown Univ., WADC TN 56-395, Providence, RI, 1956.

[44]Hornung, H. G., "Non-Equilibrium Dissociating Nitrogen Flow over Spheres and Circular Cylinders," *Journal of Fluid Mechanics*, Vol. 53, Pt. 1, 1972, pp. 149–176.

[45]Hornung, H. G., and Wen, C.-Y., "Nonequilibrium Dissociating Flow over Spheres," AIAA Paper 95-0091, Jan. 1995.

[46]Chung, P. M., "Chemically Reacting Nonequilibrium Boundary Layers," *Advances in Heat Transfer*, edited by J. P. Hartnett and T. F. Irvine Jr., Vol. 2, Academic, New York, 1965.

[47]Goulard, R., " On Catalytic Recombination Rates in Hypersonic Stagnation Heat Transfer," *Jet Propulsion*, Vol. 28, Nov. 1958, pp. 737–745.